Undercatch Adjustments for Tipping-Bucket Gauge Measurements of Solid Precipitation

JOHN KOCHENDORFER,[a] MICHAEL E. EARLE,[b] DANIEL HODYSS,[c] AUDREY REVERDIN,[d] YVES-ALAIN ROULET,[e] RODICA NITU,[f] ROY RASMUSSEN,[g] SCOTT LANDOLT,[g] SAMUEL BUISÁN,[h] AND TIMO LAINE[i]

[a] *Atmospheric Turbulence and Diffusion Division, NOAA/ARL, Oak Ridge, Tennessee*
[b] *Meteorological Service of Canada, Environment and Climate Change Canada, Dartmouth, Nova Scotia, Canada*
[c] *Remote Sensing Division, Naval Research Laboratory, Washington, D.C.*
[d] *Swiss Federal Institute of Technology Lausanne, Lausanne, Switzerland*
[e] *Meteoswiss, Payerne, Switzerland*
[f] *Environment and Climate Change Canada, Toronto, Ontario, Canada*
[g] *National Center for Atmospheric Research, Boulder, Colorado*
[h] *Delegación Territorial de AEMET en Aragón, Zaragoza, Spain*
[i] *Finnish Meteorological Institute, Helsinki, Finland*

(Manuscript received 31 October 2019, in final form 6 April 2020)

ABSTRACT

Heated tipping-bucket (TB) gauges are used broadly in national weather monitoring networks, but their performance for the measurement of solid precipitation has not been well characterized. Manufacturer-provided TB gauges were evaluated at five test sites during the World Meteorological Organization Solid Precipitation Intercomparison Experiment (WMO-SPICE), with most gauge types tested at more than one site. The test results were used to develop and evaluate adjustments for the undercatch of solid precipitation by heated TB gauges. New methods were also developed to address challenges specific to measurements from heated TB gauges. Tipping-bucket transfer functions were created specifically to minimize the sum of errors over the course of the adjusted multiseasonal accumulation. This was based on the hypothesis that the best transfer function produces the most accurate long-term precipitation records, rather than accurate catch efficiency measurements or accurate daily or hourly precipitation measurements. Using this new approach, an adjustment function derived from multiple gauges was developed that performed better than traditional gauge-specific and multigauge catch efficiency derived adjustments. Because this new multigauge adjustment was developed using six different types of gauges tested at five different sites, it may be applicable to solid precipitation measurements from unshielded heated TB gauges that were not evaluated in WMO-SPICE. In addition, this new method of optimizing transfer functions may be useful for other types of precipitation gauges, as it has many practical advantages over the traditional catch efficiency methods used to derive undercatch adjustments.

1. Introduction

Precipitation is a vital component of meteorology, hydrology, and climate, and there is significant uncertainty regarding how precipitation will change with Earth's climate (Greve et al. 2014; Trenberth 2011; Trenberth et al. 2003). Many regions already experience agricultural and municipal water shortages, and globally, uncertainty and scarcity in available water are expected to rise (Schewe et al. 2014). In addition, the spatial extent of areas prone to drought and vulnerability to flooding are both increasing (Hirabayashi et al. 2013; Huang et al. 2015). For these reasons, accurate precipitation measurements are needed by watershed managers, hydrologists, emergency management agencies, meteorologists, and climatologists. Solid precipitation measurements, in particular, are subject to large measurement errors, due primarily to undercatch caused by wind (Fortin et al. 2008;

Denotes content that is immediately available upon publication as open access.

Supplemental information related to this paper is available at the Journals Online website: https://doi.org/10.1175/JHM-D-19-0256.s1.

Corresponding author: John Kochendorfer, john.kochendorfer@noaa.gov

DOI: 10.1175/JHM-D-19-0256.1

Goodison et al. 1998; Goodison 1978; Rasmussen et al. 2012; Sugiura et al. 2003; Thériault et al. 2012; Wolff et al. 2013). Additional uncertainty may result from snowfall collecting on the gauge and drifting snow accumulating within wind shields, either of which can completely or partially block the gauge inlet. Further, the accuracy of solid precipitation measurements is limited by the precision and resolution required to measure the low precipitation rates typically associated with snowfall. Prompted by these challenges and an increase in the prevalence of automated solid precipitation measurements (Nitu and Wong 2010), the World Meteorological Organization facilitated the Solid Precipitation Intercomparison Experiment (WMO-SPICE) to evaluate instruments for the measurement of precipitation and make recommendations for their implementation, among other objectives (Nitu et al. 2018).

Weighing precipitation gauges are typically recommended for the measurement of solid precipitation. This view was supported by the measurements recorded and presented in the previous WMO Solid Precipitation Measurement Intercomparison (Goodison et al. 1998), and it was reinforced by the results of the more recent WMO-SPICE (Nitu et al. 2018). Weighing precipitation gauges have several significant advantages over tipping-bucket (TB) gauges for the measurement of solid precipitation. The response time of a weighing gauge is typically better than that of a TB gauge, as solid precipitation must be melted within the funnel of a TB gauge before being measured. In addition, TB precipitation gauges only report after a full tip of water has accumulated (typically 0.1–0.2 mm). Such measurement delays are more significant for snowfall than for rain, partly because of the typically low precipitation rates associated with snowfall (e.g., Boudala et al. 2017). Therefore, TB gauges cannot be used to accurately determine the timing of precipitation events (Nitu et al. 2018; Savina et al. 2012). Like weighing gauges, TB gauges also experience undercatch due to wind (Buisán et al. 2017, hereafter B17; Duchon et al. 2014; Savina et al. 2012). In addition, TB gauges may underestimate solid precipitation due to the removal of snow by wind (scouring) from the gauge funnel and evaporation from both the funnel and the tipping bucket (Savina et al. 2012).

One key advantage of using heated TB gauges instead of weighing gauges, however, is initial cost, as TB gauges are typically less expensive to purchase than weighing gauges. In addition, weighing gauges are subject to measurements noise that can produce false precipitation reports, which may require auxiliary measurements and sophisticated algorithms to address (e.g., Leeper et al. 2015; Wolff et al. 2015; Smith et al. 2019a). Although TB gauges have significant maintenance requirements, as long as they remain unclogged by debris they have an unlimited capacity, as precipitation is measured and flows out of the gauge, whereas weighing gauge buckets collect precipitation and must be emptied periodically as they approach their maximum capacity. Oil and antifreeze are not required for TB gauges, but are recommended for use in weighing gauge buckets to prevent freezing and evaporation of both water and antifreeze. The use of oil and antifreeze also presents additional challenges. For example, they require proper transportation and storage both before and after their use, and may be prohibited or subject to additional environmental assessments in some protected areas. For these reasons, and because historically TB were the first gauges available for automated precipitation measurements, TBs are the most widely used automated precipitation gauges despite their limitations for snowfall measurements (Nitu and Wong 2010). Because of this widespread use, adjustments are needed to help improve the shortcomings of TB gauge measurements. The WMO-SPICE TB gauge measurements are well suited to develop such adjustments, due to the high quality of the measurements, the availability of a solid precipitation measurement reference, and the number of sites and gauges included in the intercomparison.

A large body of work has been dedicated to the evaluation of the accuracy of TB measurements of liquid precipitation (e.g., Ciach 2003; Sypka 2019), some of which was performed in previous WMO intercomparisons (Lanza et al. 2005; Lanza and Vuerich 2009; Sevruk et al. 2009). For rainfall, the effects of wind on TB gauges have been described using numerical simulations, which compared well to wind tunnel and field measurements (Nešpor and Sevruk 1999). Previous work in both the laboratory and the field has also demonstrated that TB gauges underestimate liquid precipitation falling at high rates and in high wind conditions (Duchon et al. 2014, 2017). The effects of high rainfall rates on TB measurements have been well characterized using dynamic laboratory calibrations; corrections have been developed to compensate for resulting measurement underestimates (e.g., Lanza and Stagi 2012).

New undercatch adjustments, referred to more generally as transfer functions, have been developed recently for weighing gauges. Wolff et al. (2015) derived a transfer function for a single Alter shielded weighing gauge using measurements from a Norwegian site. They used Bayesian analysis to determine the most appropriate form of an adjustment that described undercatch as a sigmoidal function of both air temperature T_{air} and wind speed U. As is typical for this type of work, the gauge catch efficiency (CE) was calculated as the ratio

of the amount of precipitation recorded by the gauge under evaluation, divided by the amount of precipitation recorded by a reference over a specified time period.

In an effort to create broadly applicable adjustments, and also to quantify the uncertainty associated with the use of a single transfer function at multiple sites, multisite transfer functions were derived using WMO-SPICE weighing gauge measurements (Kochendorfer et al. 2017b). More recent work based on WMO-SPICE measurements demonstrated that adjustments derived using one type of weighing gauge can be used effectively on other types of weighing gauges with the same unshielded or shielded configuration (Kochendorfer et al. 2018). This work identified the presence or type of wind shield as the most significant determinant of gauge undercatch.

Despite their broad use, the undercatch of heated TB gauges is not as well characterized as that of weighing gauges. Because TB gauges must collect and then melt precipitation before recording it, their undercatch may be more sensitive to the specific site, hydrometeor type, and precipitation rate than weighing gauges. Likewise, variations in funnel depths, inlet sizes, materials, and heating may also affect the amount of solid precipitation that is collected by different types of TB gauges. Accordingly, TB gauge adjustments may be more gauge specific than weighing gauge adjustments.

B17 evaluated the performance of a heated TB gauge (Precipitation Transmitter, Thies Clima, Germany) for the measurement of solid precipitation at the WMO-SPICE site in the Spanish Pyrenees mountains. Using a transfer function derived as a function of wind speed, temperature and precipitation intensity this work demonstrated that the accumulation of (primarily solid) precipitation over the course of a winter season could be recorded accurately using a heated TB gauge with an appropriate adjustment. An evaluation of the same gauge and site used by B17 was included in the WMO-SPICE final report. Five other types of heated TB precipitation gauges were also evaluated at four additional WMO-SPICE sites (Nitu et al. 2018). The WMO-SPICE report included a thorough examination of the strengths, weaknesses, errors, and other issues regarding heated TB solid precipitation measurements, but it did not include the derivation of undercatch adjustments.

The primary objective of this work is to derive transfer functions to ameliorate the effects of undercatch for heated TB solid precipitation measurements using the WMO-SPICE dataset. In the interest of producing more broadly applicable adjustments, with representative uncertainties, the application of a single function to measurements from multiple sites was investigated. Because WMO-SPICE included several different types of TB gauges, both gauge-specific and multigauge transfer functions were also derived.

2. Methods

a. Precipitation measurements

Heated TB gauges were evaluated at five WMO-SPICE test sites: the Canadian CARE site (CARE), the Swiss Weissfluhjoch site (Weis), the Finnish Sodankylä site (Sod), the Spanish Formigal site (For), and the U.S. Marshall site (Ma). Site locations are shown in Fig. 1 and are described in detail in the WMO-SPICE commissioning reports (available here: http://www.wmo.int/pages/prog/www/IMOP/intercomparisons/SPICE/SPICE.html). Background information such as site elevation, mean winter (1 October–30 April) precipitation, and statistics describing the air temperature and wind speed during precipitation events are included in Table 1.

Six unshielded TB gauge models were evaluated in WMO-SPICE over the 2013/14 and 2014/15 winter seasons (Table 2). The CAE PMB25R (from CAE S.p.A., San Lazzaro di Savena, Italy, hereafter referred to as the CAE) was installed at CARE and Marshall. Two different Meteoservis MR3H-FC gauge models were evaluated. One was the MR3H-FC (Meteoservis, Vodňany Czech Republic, hereafter MR3H), which was installed at CARE, Marshall, and Sodankylä. The other gauge was made specifically for the Austrian Central Institute for Meteorology and Geodynamics (ZAMG, hereafter the ZAMG MR3H), and was evaluated at CARE and Weissfluhjoch. Two different models of the Thies Precipitation Transmitter were tested. The Model 5.4032.35.228 was tested at Formigal. This model is used by the Spanish Meteorological Agency (AEMET) and has a 0.2-mm resolution and 49-W heating output. The Thies Model 5.4032.45.008 was tested at Marshall, was heated with 113 W, and had a 0.1-mm resolution. The Hydrological Services America (HSA) TBH (from Hydrological Services America, Lake Worth, Florida, United States, hereafter referred to as the HSA) was installed at CARE and Marshall. To conserve power, the HSA gauge heater is activated by the presence of snow in the funnel. This makes the HSA appropriate for use in remote locations, where power is limited. However, the HSA gauge is also subject to longer measurement delays than the other TB gauges evaluated (Nitu et al. 2018).

All gauges report precipitation intensity based on the number of tips during the sampling period, which was 1 min at all sites except Marshall, where the test gauges were sampled at 6-s intervals. With the exception of the HSA, all gauges performed an internal intensity correction to compensate for kinematic effects (precipitation

FIG. 1. Map of WMO-SPICE sites where tipping-bucket precipitation gauges were evaluated.

losses between successive tips of the collection mechanism) at higher intensities.

The reference precipitation measurements were recorded using the double-fence automated reference (DFAR) configuration at each site. Each DFAR consisted of a weighing precipitation gauge (either an OTT Pluvio2, from OTT Hydromet, Kempten, Germany, or a 3-wire T-200B3, Geonor Inc., Oslo, Norway) installed with a single-Alter shield within a large, octagonal double fence (Nitu et al. 2018). Example photographs of the TB gauges and the DFAR are shown in Fig. 2. Reference measurements were recorded during both winter seasons, with the exception of the Formigal site, where the DFAR was only available for the winter of 2014/15.

b. *Ancillary measurements*

Wind speed and air temperature were recorded at all sites, typically using instrumentation favored by the host country/institute. Wind speed was recorded at gauge height and/or at 10 m. However, at most of the sites where it was recorded at both heights, one height was found to be more representative of the site wind speed. This was due to isolated obstructions at gauge height or the presence of trees surrounding the site. To derive transfer functions for both the gauge and 10-m-height wind speeds, an estimate of wind speeds at both heights were required from every site. Using the methods described in Kochendorfer et al. (2017b), when only one representative wind speed measurement height was available, the logarithmic wind profile was relied upon to scale measurements recorded at 10 m to gauge height, or vice versa.

c. *Data quality control*

Precipitation and ancillary meteorological measurements from all sites were submitted to a central repository hosted by the U.S. National Center for Atmospheric Research (NCAR). Data from all sensors and sites were quality controlled and processed using standardized methods. The TB and DFAR precipitation measurements were subject to a set of range and jump checks to remove erroneous values. In addition, a Gaussian filter was applied to reduce high-frequency noise in the DFAR data. An independent precipitation detector (Laser Precipitation Monitor, Thies Clima, Germany or Parsivel^2, OTT Hydromet, Germany) was used at each site to help ensure that the DFAR weighing gauge measurements coincided with periods of precipitation, and were not the result of measurement artifacts. These data quality control and processing methods are summarized in Kochendorfer et al. (2017b) and described in greater detail in Reverdin et al. (2016) and Nitu et al. (2018).

The air temperature and wind speed measurements were also checked for validity, with missing or suspect measurements excluded from the analysis. Wind speeds equal to 0 m s^{-1} were excluded from the analysis, as it

TABLE 1. Descriptions of WMO-SPICE test sites, including the site abbreviation (Abbr), country, elevation, latitude, mean gauge-height wind speed U_{gh}, the gauge height Z_{gh}, mean air temperature T_{air}, and mean total winter (1 Oct–30 Apr) precipitation recorded by the DFAR from each site over the 2013/14 and 2014/15 winter seasons. Wind speed and air temperature statistics were calculated for precipitation events only, and therefore differ from normal annual site climatologies.

Site Abbr	Country	Elev (m)	Lat	Mean U_{gh} (m s^{-1})	Z_{gh} (m)	Mean T_{air} (°C)	Mean P (mm)
CARE	Canada	251	44.23°	3.2	1.5	−3.3	186
Sod	Finland	179	67.37°	1.6	1.4	−2.1	234
Weis	Switzerland	2537	46.83°	3.8	3.5	−7.2	377
For	Spain	1800	42.76°	2.3	1.5	−0.7	321
Ma	United States	1742	39.59°	2.8	1.7	−2.0	236

TABLE 2. Tipping-bucket gauges, the WMO-SPICE sites where they were evaluated, their measurement resolution, their collection area, and the number of days with precipitation (P days) available for each gauge.

Sensor	Site(s)	Resolution (mm)	Collection area (cm^2)	P days
CAE PMB25R	CARE, Marshall	0.1	1000	175
Hydrological Services America (HSA) TBH	CARE, Marshall	0.2	314.15	174
Meteoservis MR3H-FC	CARE, Marshall, Sodankylä	0.1	500	358
Meteoservis MR3H-FC, ZAMG	CARE, Weissfluhjoch	0.1	500	118
Thies Precipitation Transmitter, model 5.4032.35.228	Formigal	0.2	200	52
Thies Precipitation Transmitter, model 5.4032.45.008	Marshall	0.1	200	80

was difficult to determine whether these were valid measurements or the result of a mechanical failure or a frozen anemometer. The WMO-SPICE sites were all designed to minimize the effects of cross interference between the measurements and unintended wind blockage from different structures and wind shields. This was done based on the primary wind directions associated with winter precipitation. At some sites, however, such interference still may have occurred, and potentially affected measurements were excluded from the analysis using the methods described in Kochendorfer et al. (2017b).

d. Catch efficiency transfer functions

1) TRANSFER FUNCTION DEVELOPMENT

Transfer functions are typically derived from catch efficiency measurements, with catch efficiency defined as the ratio of the amount of precipitation caught in the gauge under test to that caught by the reference configuration:

$$\mathrm{CE} = \frac{P_{\mathrm{UT}}}{P_{\mathrm{Ref}}}, \tag{1}$$

where CE is catch efficiency, P_{UT} is the precipitation amount from the gauge under test, and P_{Ref} is the reference precipitation amount. CE is calculated for defined time periods, with different researchers typically using accumulation time periods between 30 min and 24 h, depending on the type of precipitation measurement and the intended use of the transfer function. The form of the CE transfer function used in this work is given in Eq. (2):

$$\mathrm{CE} = (a)e^{-b(U)}, \tag{2}$$

where U is the wind speed, and a and b are coefficients fit to the measurements. This equation was fit separately to mixed and solid precipitation, with solid precipitation defined as occurring when $T_{\mathrm{air}} < -2°\mathrm{C}$, and mixed precipitation defined as occurring when $2° \geq T_{\mathrm{air}} \geq -2°\mathrm{C}$. An alternative, more complex form of the transfer function from Kochendorfer et al. (2017a) that includes T_{air} was also tested with these TB measurements, but it did not perform better than creating separate transfer functions for mixed and solid precipitation.

2) EVENT SELECTION

In the interest of producing representative transfer functions, measurements used to derive CE were selected with great care. Precipitating periods when a TB

FIG. 2. Examples of the CAE, HSA, MR3H, Thies, and DFAR precipitation gauges (from left to right).

gauge accumulated no precipitation were common due to TB measurement delays (section 1), particularly during periods of light precipitation, at the beginning of precipitation events, and for events with durations shorter than typical TB response delays. Such periods were included in the data used to derive CE transfer functions, because excluding them resulted in biased CE values. In addition, only events with more than some minimum amount of precipitation caught by the DFAR were included in the dataset. For 30-min and 1-, 3-, and 6-h event datasets, this DFAR threshold was 0.25 mm, and for the 12- and 24-h periods, it was 1.0 mm (Kochendorfer et al. 2017a,b). This helped decrease the root-mean-square error (RMSE) of the transfer function and ensure that precipitation was actually occurring during the periods included in the CE transfer functions.

3) Combining datasets for multisite and multigauge transfer functions

Gauge-specific CE transfer functions were fit to data from all sites at which a given gauge was tested; with the exception of the two Thies gauges, measurements from at least two sites were combined into each set of gauge-specific CE measurements. Due to differences in heating algorithms, the MR3H and the ZAMG MR3H were treated as two separate gauges. The two different Thies CLIMA tipping-bucket gauge models tested had different specifications (bucket capacity, heating power) to meet different operational requirements, and were also treated as two separate gauges.

For weighing gauges, it has been demonstrated that the primary determinant of undercatch, and, therefore, the transfer function, is the type of wind shield, or the lack of a wind shield, rather than the specific model of weighing gauge (Kochendorfer et al. 2018). To determine if this is also true for TB gauges, a multigauge transfer function was derived, in addition to gauge-specific transfer functions. The coefficients of the multigauge transfer function were fit to all of the available TB gauge measurements, from all of the available sites, rather than just one type of TB gauge available at its respective sites. The HSA measurements, however, were excluded from the derivation of the multigauge function. This was due to significant differences in the operating principles of the HSA gauge that help conserve power, but also cause significantly more delayed precipitation measurements. The multigauge transfer function was evaluated alongside the transfer functions that were custom fit to each type of TB gauge.

4) Issues related to CE-based transfer functions

For weighing gauges, the CE approach for transfer function derivation presents challenges due to measurement noise, making it difficult to determine an appropriate minimum amount of measurable precipitation. In addition, analysis methods used to produce precipitation records typically conserve precipitation accumulated below the measurement threshold, but such low-rate precipitation cannot be used to derive CE and transfer functions due to the constraints of using a ratio. To ensure that the measurements used to calculate CE are representative, the minimum threshold and accumulation time period must be chosen carefully.

It is particularly difficult to derive representative CE functions for heated TB gauges, because of their inherent response delays. For example, time series of accumulated precipitation from TB gauges and a DFAR are shown in Fig. 3. For over an hour after the DFAR began accumulating precipitation, none of the TB gauges reported any precipitation, which would result in a CE of zero during this initial period. It is also difficult to include precipitation that is recorded by a TB gauge after an event has ended, as a value of 0.0 mm recorded by the reference gauge cannot be include in the denominator of a CE value. The HSA shown in Fig. 3 provides an example of this, as it reported precipitation during a pause in the event, at about 1930 local time. Although such delays were more prevalent with the HSA gauges, all of the TB gauges evaluated were subject to delays (Nitu et al. 2018).

Due to the effects of such measurement delays, the TB transfer functions derived from CE measurements were very sensitive to the accumulation time period used to calculate CE. To illustrate this sensitivity, transfer functions derived using different accumulation time periods for the CAE gauge are shown in Fig. 4. The inclusion of periods with zero TB precipitation made the transfer functions less sensitive to the accumulation time period, but they still differed significantly from each other. Unfortunately, it was difficult to determine which function would be the most accurate and broadly applicable for long-term measurements. This is one of the reasons that an alternative to the typical CE-based transfer function derivation was needed.

e. Cumulative seasonal approach

One fundamental issue with the classical, CE-based derivation method is that transfer functions are optimized to minimize errors in CE, rather than errors in adjusted precipitation measurements. This may be problematic, given that the objective of a transfer function is to produce more accurate precipitation measurements, not accurate CE values. Therefore, a more direct method for the derivation of transfer functions was developed. The first, and most critical, step to the new approach was to determine the best way to assess the transfer function.

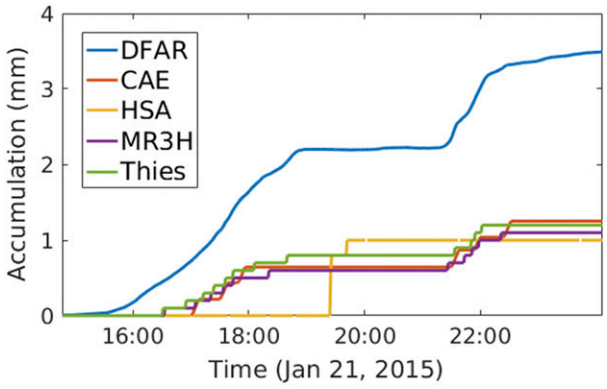

FIG. 3. Example time series of tipping-bucket precipitation gauge accumulations from the Marshall testbed.

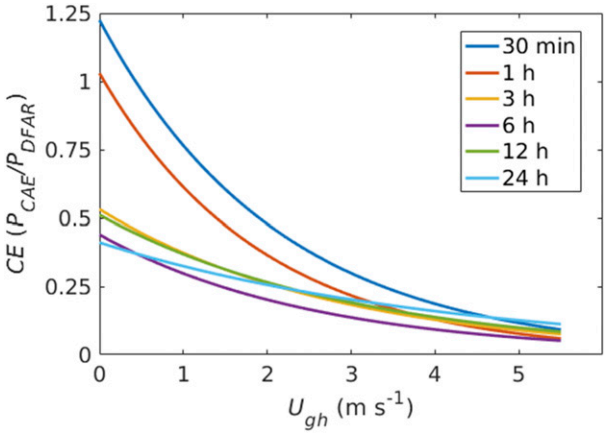

FIG. 4. Catch efficiency curves derived using precipitation events with different durations. Precipitation measurements are from the CAE tipping-bucket gauge and DFAR at CARE and Marshall, and are compared to the gauge-height wind speed U_{gh}.

The RMSE and the total bias of adjusted measurements relative to the DFAR measurements were both viable metrics available for transfer functions testing. However, transfer functions can also be evaluated based on cumulative errors in adjusted accumulation relative to the reference values at specified intervals (e.g., hourly) over the duration of a measurement season (Smith et al. 2019b).

Figure 5 demonstrates the use of such long-term accumulation time series for transfer function evaluation. All of the CAE solid and mixed precipitation measurements recorded at CARE over two winter seasons were adjusted using the CE transfer functions shown in Fig. 4. In this example, the function derived from the 30-min events was shown to be the most suitable for this set of CAE precipitation measurements, because it produced an adjusted accumulation that was closest to that of the DFAR throughout both winter seasons. This was unexpected, because of the unrealistically high a coefficient of the CAE 30-min transfer function (Fig. 3), and because 30 min is too short of a time period to be used for TB transfer functions. Typical response times for these TB gauge measurements were about 40 min, and it is recommended that the assessment interval should be selected to exceed the response time in order to mitigate the influence of missed reports (Nitu et al. 2018). As described in more detail below, such cumulative seasonal accumulations can also be used to develop new transfer functions, by optimizing the parameters of an existing transfer function to minimize the sum of differences between the seasonal time series of cumulative adjusted precipitation measurements and cumulative DFAR measurements.

One of the advantages of this cumulative seasonal approach is that it included all of the recorded precipitation measurements, mimicking an operational TB gauge. Because this evaluation was not directly dependent on CE, periods when the DFAR or the gauge under evaluation caught zero precipitation could all be included in the assessment, making it a more representative and ''true-to-life'' test of transfer functions. Further, seasonal accumulation totals for solid precipitation are critical for hydrology and flood forecasting; in many networks, one of the primary purposes of monitoring solid precipitation is to determine seasonal totals.

Optimizing the transfer functions to minimize errors in the cumulative seasonal precipitation records produced transfer functions that were unrealistically insensitive to wind speed (Fig. 6, multigauge optimized). To retain sensitivity to wind speed, a two-step approach was also implemented: 1) a preliminary CE transfer function was determined by fitting Eq. (2) to the hourly CE measurements (Fig. 6, multigauge CE) to obtain the parameter a and a preliminary estimate of parameter b; 2) parameter b was optimized to minimize the sum of hourly errors over the entire course of the seasonal accumulation, while keeping parameter a fixed to the value found in the first step (Fig. 6, multigauge optimized with fixed intercept). Hourly measurements were used because they were short enough to allow for the calculation of representative mean air temperatures and wind speeds, but longer than the 30-min measurements that suffered more significantly from the effects of delayed TB measurements.

The hourly measurement record of every TB gauge (with the exception of the HSA gauge) was adjusted using the same multigauge transfer function. For each gauge, at each site, the total cumulative error was estimated as the mean square error of the adjusted running cumulative total TB accumulation relative to the corresponding running cumulative total DFAR accumulation:

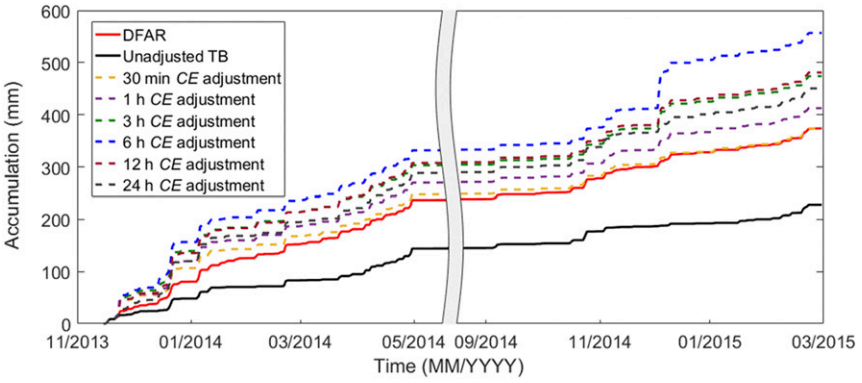

FIG. 5. Multiseason accumulation of CAE (black line) and DFAR precipitation at the Marshall site. CAE measurements adjusted using the transfer functions in Fig. 4 are also shown. Only winter (1 Oct–30 Apr) solid and mixed precipitation measurements were included in the assessment, so the warm season was excluded from the time series using a break in the x axis.

$$\mathrm{Err} = \frac{\sum_{1}^{N} [\mathrm{cumsum}(P_{\mathrm{DFAR}}) - \mathrm{cumsum}(P_{\mathrm{TB}})]^2}{N}, \quad (3a)$$

where N is the total number of hours in the dataset, P_{TB} is the hourly tipping-bucket precipitation, P_{DFAR} is the hourly DFAR precipitation, and

$$\mathrm{cumsum}(P, M) = \sum_{1}^{M} P. \quad (3b)$$

In Eq. (3b) cumsum describes the running cumulative sum of the hourly precipitation measurements, where P is the hourly precipitation and M is not the total number of hours, but the Mth hourly value of the time series. In Eq. (3a), the cumsum function is used to derive the total seasonal DFAR and TB accumulations at each of M hourly intervals, and then calculate the average squared error over all N intervals. For example, for one of the adjustments shown in Fig. 5, the Err described in Eq. (3a) would be calculated from the differences between the adjusted TB curve and the corresponding DFAR curve, over the course of the entire record, for every available hourly measurement. Treating the solid and mixed precipitation separately, the error was calculated for each adjusted gauge, at each site. Coefficient b in Eq. (2) was then found by minimizing Eq. (3a) using the Nelder–Mead simplex method (Nelder and Mead 1965) with the initial starting value for the optimization set to the value of b determined in the first step using hourly CE measurements.

f. Transfer function evaluation

The different transfer functions were evaluated by applying them to hourly TB gauge measurements; solid and mixed precipitation measurements were adjusted separately using the appropriate adjustments, and liquid precipitation was excluded from the evaluation. Total daily accumulations were then calculated. The RMSE was calculated, with the error estimated as the difference between the daily (un)adjusted TB measurements and the corresponding DFAR measurement. The correlation coefficient (r) between the adjusted TB measurements and the corresponding (daily) DFAR precipitation accumulation was also calculated. The percentage of daily precipitation totals with errors smaller than 1.0 mm ($\mathrm{PE}_{1.0\mathrm{mm}}$) of the daily precipitation totals were calculated,

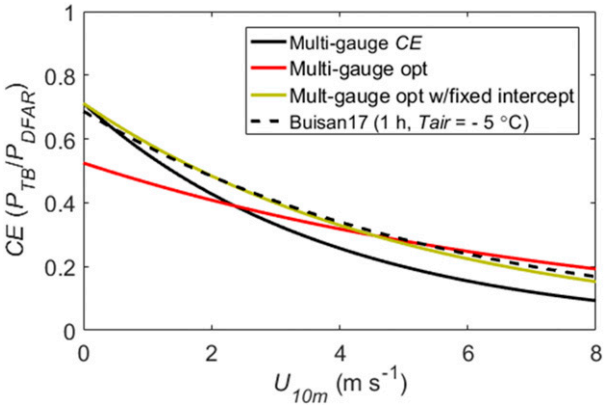

FIG. 6. Comparison of multigauge solid precipitation transfer functions, and a transfer function from B17. The function derived from hourly CE (multigauge CE, black line), the function derived by optimizing the function to minimize errors in the seasonal accumulation (multigauge opt, red line), and the hybrid function (multigauge optimized with fixed intercept, yellow line) that was optimized to minimize errors in the seasonal accumulation with the fixed intercept [parameter a from Eq. (2)] from the CE function are shown. The B17 function derived for 1-h solid precipitation that included T_{air} as a separate variable is also shown, with $T_{\mathrm{air}} = -5$°C (B17 1 h, $T_{\mathrm{air}} = -5$°C, dashed line).

with errors estimated as the difference between the adjusted TB measurements and the DFAR measurements. This statistic was used by Kochendorfer et al. (2017b) for 30-min weighing precipitation gauge measurements, with a lower threshold (0.1 mm) used for the smaller 30-min accumulations. Following Pierre et al. (2019), the bias (Pbias) in the measurements was also estimated as a percentage of the total of the DFAR precipitation measurements:

$$\text{Pbias} = 100\% \times \frac{P_{\text{TB}}}{P_{\text{DFAR}}}, \tag{4}$$

where P_{TB} is the precipitation amount reported by the tipping-bucket gauge, and P_{DFAR} is the precipitation amount reported by the DFAR. For the sake of comparison, these error statistics were also calculated for the uncorrected measurements.

3. Results and discussion

a. Transfer functions

Unique CE transfer functions were derived for each of the TB gauge types evaluated in WMO-SPICE (gauge-specific functions). The TB measurements from all gauge types were then pooled together and used to derive a multigauge CE transfer function (Fig. 6, multigauge CE). As described in section 2e, a multigauge function optimized to minimize the sum of errors in the seasonal accumulations from all gauges, at all sites was derived (Fig. 6, multigauge opt). In addition, a similarly optimized multigauge function that was modified to produce a more realistic CE response to wind speed was derived (Fig. 6, multigauge opt w/fixed intercept).

The multigauge functions fell within the range of the different B17 functions (not shown), and the 1-h function most highly recommended from B17 [S. Buisan 2020, personal communication; $\text{CR} = 1.01 \times \exp(0.077 \times T - 0.176 \times W)$] matched the fixed-intercept optimized function remarkably well (Fig. 6). Despite differences in the derivation and application methods between these transfer functions, this suggests that both sets of transfer functions may be widely applicable. The T_{air} of −5°C was used for the comparison because this was the approximate mean T_{air} for the solid precipitation measurements in WMO-SPICE (Kochendorfer et al. 2017b).

b. Transfer function testing

Error statistics were computed for all adjusted and unadjusted measurements (Fig. 7). Correlation coefficients were near unity for all of the different adjustments; however, they were also similar for the uncorrected measurements, so this statistic was not very sensitive to differences between the adjustments. With the exception of the HSA gauges, the $\text{PE}_{1.0\text{mm}}$ was generally higher (indicating more accurate measurements) for the adjusted measurements than the unadjusted measurements. By this measure, the gauge-specific adjustments were typically less accurate than the multigauge adjustments, and the optimized functions were typically more accurate than the multigauge CE function.

The Pbias also indicated that the gauge-specific functions were less effective than the multigauge functions at minimizing the bias in the adjusted measurements; the gauge-specific functions typically overadjusted the measurements, causing a positive bias. The significant negative bias of the unadjusted measurements is also apparent in Fig. 7. As the parameters of the optimized functions were chosen to minimize cumulative errors in the seasonal course of precipitation accumulation, it is not surprising that they were typically more effective than the CE-derived functions at reducing the Pbias. In addition to having a small bias for the combined TB measurements (Fig. 7, All), these optimized functions also effectively minimized site-specific biases relative to the CE-derived functions. This was observed even for the measurements from Weissfluhjoch; previous studies showed a marked bias in weighing gauge adjustments from this alpine site with complex topography relative to other sites (Kochendorfer et al. 2017b). In addition, based on the Pbias, both of the optimized multigauge functions performed similarly. Because the fixed-intercept function was given less freedom to minimize errors in the seasonal accumulations across all gauges, at all sites, we might expect to see worse bias results relative to the original optimized function. However, this was not the case, and the fixed-intercept version of the optimized function was about as effective at reducing the bias at all of the sites as the original multigauge optimized function. This was true at the low-wind site of Sodankylä and also at the windier sites, which is noteworthy because the sensitivity of CE to wind speed was enhanced in the fixed-intercept function.

In general, the gauge-specific functions resulted in higher RMSE values than the multigauge functions. It should also be noted that the CE functions were derived not to minimize errors in adjusted precipitation measurements, but errors in CE, so it is not surprising that they were not always effective at reducing the RMSE of the adjusted measurements. The fact that the multigauge functions reduced the RMSE more than the gauge-specific functions also indicates that these different TB gauges may all be effectively adjusted using the same function. The RMSE results for both of the optimized functions were generally lower than for the CE transfer functions, and the two different optimized functions resulted in similar RMSEs for the different

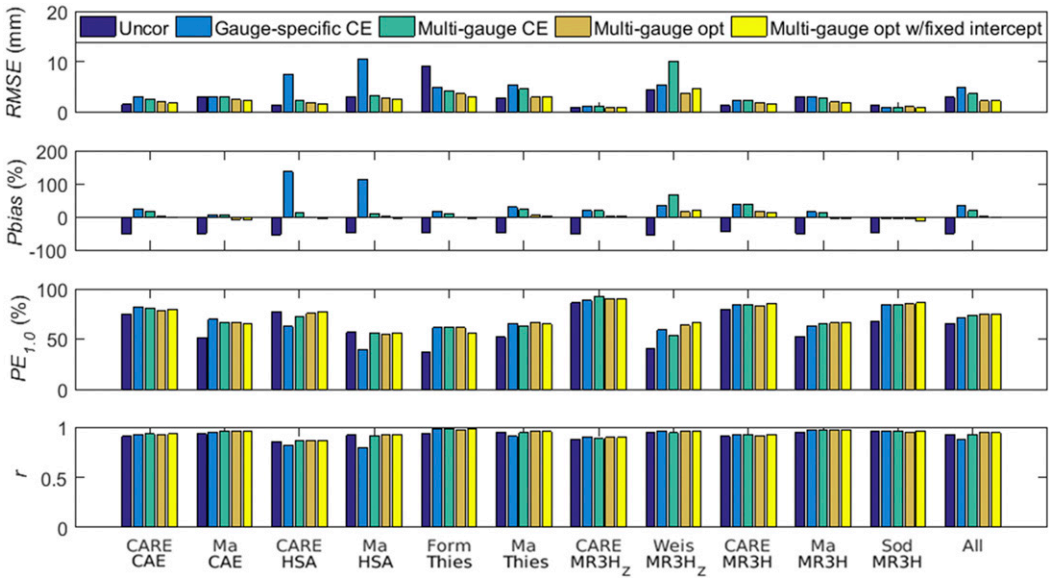

FIG. 7. RMSE, percent bias (Pbias), percent of daily events with errors less than 1.0 mm ($PE_{1.0mm}$), and correlation coefficient (r) for daily results. Uncorrected (uncor; dark blue) results are shown. Results adjusted using gauge-specific catch efficiency transfer functions (gauge-specific CE; light blue), the multigauge catch efficiency transfer function (multigauge CE; green), the multigauge optimized transfer function (multigauge opt; tan), and the multigauge optimized transfer function with the fixed intercept (multigauge opt with fixed intercept; yellow) are also shown. The ZAMG MR3H is abbreviated as $MR3H_Z$. Statistics calculated from all of the tipping-bucket measurements combined together into one dataset are also shown (all). Only gauge-height wind speed transfer functions are shown.

gauges and sites. The RMSE values for the gauge-specific HSA functions were notably high relative to those for the other TB gauges. This is because the CE approach worked especially poorly for these gauges, for which a larger proportion of measurements occurred during periods when there was no precipitation measured by the DFAR on account of longer response delays.

An example comparison between the DFAR precipitation measurements and both the unadjusted and adjusted CAE tipping-bucket measurements at CARE is shown in Fig. 8. Some overadjustment of the TB measurements was necessary to counteract periods when precipitation occurred and the TB reported no precipitation, but the multigauge CE adjustment shown in Fig. 8 resulted in a total multiseasonal accumulation that was significantly greater than the DFAR accumulation (Fig. 7, Pbias, for the CARE CAE, multigauge CE, green bar). Figure 8 also helps demonstrate how significant overestimates could cause the RMSE of the adjusted measurements (Fig. 7, RMSE, CARE CAE, multigauge CE in green) to be larger than the unadjusted RMSE (Fig. 7, RMSE, CARE CAE, uncor in dark blue). This issue is common to such adjustments, where increasing the magnitude of the measurement to account for undercatch and improve the bias and the accuracy of the seasonal accumulation can increase the magnitude of errors over shorter time scales. This has been observed previously for weighing gauge measurements in cases when the adjustment is not well suited to measurements from a given site (Kochendorfer et al. 2017b).

As an example of the multiple-season performance of the TB transfer functions, Fig. 9 shows all of the TB gauge measurements from the Marshall testbed over two winter seasons. Despite differences in heating, materials, and physical configuration, over seasonal time scales, all of the TB gauges accumulated similar amounts of precipitation (standard deviation = 6.8 mm, or 3.5% of the average total accumulation). And when adjusted using the multigauge optimized function with the fixed intercept, the TB gauges were able to accurately reproduce the DFAR accumulation (RMSE = 16.6 mm, or 4.4% of the DFAR total accumulation).

During periods when data from one of the TB gauges were not available (site maintenance, power outage, etc.), the corresponding DFAR measurements were excluded from the reference accumulation used to evaluate that specific TB gauge. For this reason, the reference accumulation was determined separately for each TB gauge. For the sake of clarity in Fig. 9, the average of these different reference accumulations is shown. Because of this,

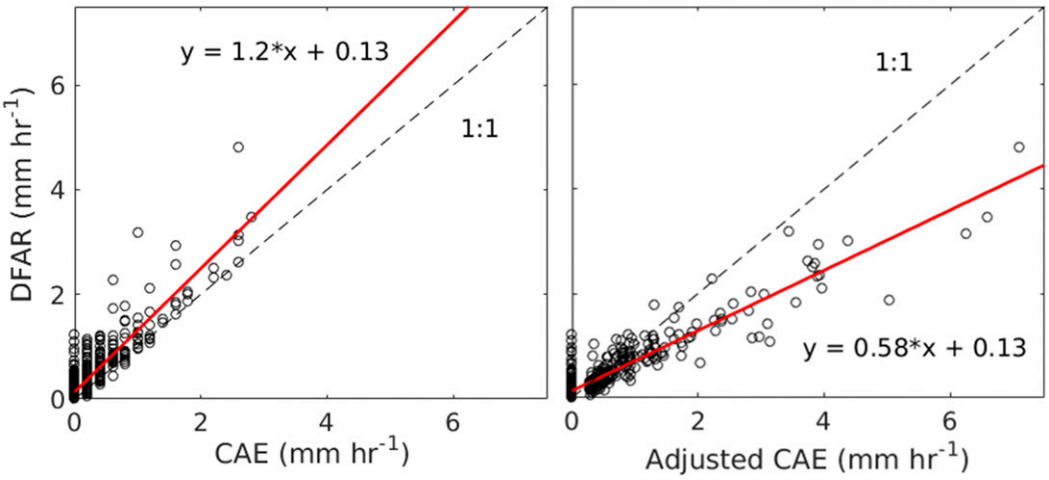

FIG. 8. Example comparison of 1-h adjusted and unadjusted CAE precipitation measurements relative to the corresponding DFAR measurements from CARE. The multigauge CE function was used for the adjustment.

the results shown in Fig. 9 differ slightly from the results shown in Fig. 7. This is only potentially apparent in the Pbias values in Fig. 7. At Marshall, the differences between the reference accumulations for different TB gauges were quite small; the reference accumulation shown in Fig. 9 was within 1% of the value of the different reference accumulations derived for all the different TB gauges at the Marshall testbed, and the difference between the maximum and minimum reference accumulations was 6.1 mm, or 1.6% of the average total accumulation.

c. *Transfer function application*

We recommend the multigauge optimized transfer function with the fixed intercept for general use with heated TB precipitation gauges. This transfer function was more realistic with respect to wind speed than the purely optimized function. It also accurately reproduced the total winter DFAR precipitation for all gauges tested, at all sites (Fig. 7, Pbias). This adjustment generally performed well based on the other evaluated error statistics, as well (Fig. 7, RMSE, $PE_{1.0}$, and r). Ideally, this transfer function should be applied to hourly precipitation measurements, using the mean hourly air temperature to determine the precipitation type, and the mean hourly wind speed to determine the magnitude of the adjustment. When applying the adjustment, the tipping-bucket measured precipitation must be divided by the CE predicted by the function. Only results for gauge-height wind speed transfer functions were shown here, but like the WMO-SPICE weighing gauge transfer functions (Kochendorfer et al. 2017b), the 10-m height wind speed transfer functions performed similarly to the gauge height transfer functions for the TB gauges

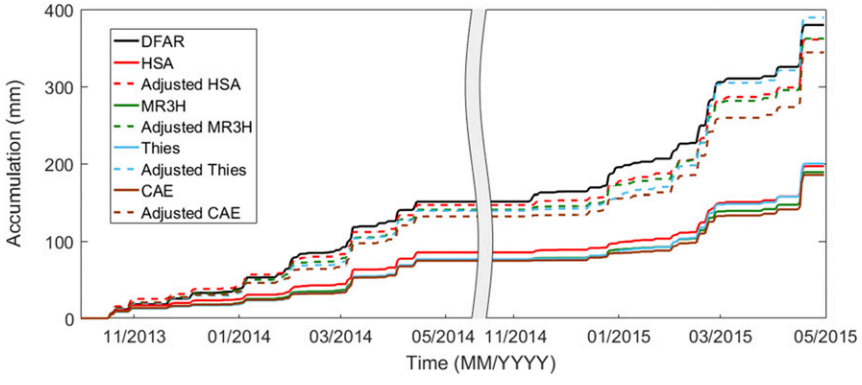

FIG. 9. Unadjusted (solid lines) and adjusted (dashed lines) tipping-bucket precipitation accumulations from the Marshall testbed over the period from October 2013 to May 2015. Only winter (1 Oct–30 Apr) mixed and solid precipitation measurements were included in the assessment, so the warm season was excluded from the time series using a break in the x axis.

TABLE 3. Recommended heated tipping-bucket transfer functions. Functions are available for both gauge height and 10-m height wind speeds. Solid ($T_{air} < -2°C$), and mixed ($2° \geq T_{air} \geq -2°C$) precipitation must be adjusted separately.

	Eq. (2), $f(U$, mixed)		Eq. (2), $f(U$, solid)		
Wind speed	a	b	A	b	U_{thresh} (m s^{-1})
$f(U_{GH})$	0.726	0.0495	0.701	0.227	6.1
$f(U_{10m})$	0.722	0.0354	0.7116	0.1925	8

(Fig. S1 in the online supplemental material). Both forms of the function are available in Table 3, along with the maximum wind speed below which they are valid. For wind speeds greater than the specified maximum wind speed, the CE value determined using the maximum wind speed should be applied.

4. Conclusions

Transfer functions for the adjustment of both mixed and solid precipitation were derived using TB gauge measurements from five WMO-SPICE sites, over the span of two winter seasons. Gauge-specific transfer functions were derived, in addition to multigauge functions. Based on the error statistics, the multigauge functions, derived from measurements combined from all gauges, at all sites, performed better than gauge-specific functions. This indicates that one transfer function can be used to adjust measurements from different types of heated TB gauges.

Functions optimized to reduce errors in the cumulative seasonal precipitation records were more accurate than functions derived directly from catch efficiency, as demonstrated by lower RMSE values and smaller biases. A hybrid-type function, derived by partially optimizing a catch efficiency derived function, was more realistic with respect to wind speed than an entirely optimized function. This hybrid, fixed-intercept, optimized function performed as well as the purely optimized function in terms of reducing the adjusted measurement errors and minimizing the biases at all of the individual sites.

The optimization method allowed for the inclusion of all precipitation measurements from TB gauges, whereas the CE approach was limited to periods during which the TB gauge and the reference both report precipitation. The optimization-based, cumulative seasonal approach, therefore, accounted for the response delays inherent to TB gauge measurements of solid precipitation, resulting in more inclusive and representative transfer functions. In addition, the new method created transfer functions that minimized errors in precipitation, which was more direct and appropriate than creating transfer functions that minimize errors in CE. This approach lends itself well to operational applications, where every snowfall measurement from a gauge must be adjusted and contributes to the seasonal total, and may be applicable to other precipitation measurements (e.g., from weighing gauges) or time scales.

Acknowledgments. The authors thank Hagop Mouradian from Environment and Climate Change Canada for contributing the mapped site locations (Fig. 1). We thank the manufacturers that provided many of the sensors used to produce these results. We also thank the World Meteorological Organization for supporting this intercomparison, and Maggie Robinson from the National Oceanic and Atmospheric Association for providing editorial comments and references.

Many of the results presented in this work were obtained as part of WMO-SPICE, conducted on behalf of the World Meteorological Organization (WMO) Commission for Instruments and Methods of Observation (CIMO). The analysis and views described herein are those of the authors, and do not necessarily represent the official outcome of WMO-SPICE. Mention of commercial companies or products is solely for the purposes of information and assessment within the scope of the present work, and does not constitute a commercial endorsement of any instrument or instrument manufacturer by the authors, NOAA, or the WMO.

REFERENCES

Boudala, F. S., G. A. Isaac, P. Filman, R. Crawford, D. Hudak, and M. Anderson, 2017: Performance of emerging technologies for measuring solid and liquid precipitation in cold climate as compared to the traditional manual gauges. *J. Atmos. Oceanic Technol.*, **34**, 167–185, https://doi.org/10.1175/JTECH-D-16-0088.1.

Buisán, S. T., M. E. Earle, J. L. Collado, J. Kochendorfer, J. Alastrué, M. Wolff, C. D. Smith, and J. I. López-Moreno, 2017: Assessment of snowfall accumulation underestimation by tipping bucket gauges in the Spanish operational network. *Atmos. Meas. Tech.*, **10**, 1079–1091, https://doi.org/10.5194/amt-10-1079-2017.

Ciach, G. J., 2003: Local random errors in tipping-bucket rain gauge measurements. *J. Atmos. Oceanic Technol.*, **20**, 752–759, https://doi.org/10.1175/1520-0426(2003)20<752:LREITB>2.0.CO;2.

Duchon, C., C. Fiebrich, and D. Grimsley, 2014: Using high-speed photography to study undercatch in tipping-bucket rain gauges. *J. Atmos. Oceanic Technol.*, **31**, 1330–1336, https://doi.org/10.1175/JTECH-D-13-00169.1.

Duchon, C. E., C. A. Fiebrich, and B. G. Illston, 2017: Observing the May 2015 record rainfall at Norman, Oklahoma, using various methods. *J. Hydrometeor.*, **18**, 3043–3049, https://doi.org/10.1175/JHM-D-17-0137.1.

Fortin, V., C. Therrien, and F. Anctil, 2008: Correcting wind-induced bias in solid precipitation measurements in case of

limited and uncertain data. *Hydrol. Processes*, **22**, 3393–3402, https://doi.org/10.1002/hyp.6959.

Goodison, B. E., 1978: Accuracy of Canadian snow gauge measurements. *J. Appl. Meteor.*, **17**, 1542–1548, https://doi.org/10.1175/1520-0450(1978)017<1542:AOCSGM>2.0.CO;2.

——, P. Y. T. Louie, and D. Yang, 1998: WMO solid precipitation measurement intercomparison. Instruments and Observing Methods Rep. 67, WMO/TD-872, 212 pp, http://www.wmo.int/pages/prog/www/IMOP/publications/IOM-67-solid-precip/WMOtd872.pdf.

Greve, P., B. Orlowsky, B. Mueller, J. Sheffield, M. Reichstein, and S. I. Seneviratne, 2014: Global assessment of trends in wetting and drying over land. *Nat. Geosci.*, **7**, 716–721, https://doi.org/10.1038/ngeo2247.

Hirabayashi, Y., R. Mahendran, S. Koirala, L. Konoshima, D. Yamazaki, S. Watanabe, H. Kim, and S. Kanae, 2013: Global flood risk under climate change. *Nat. Climate Change*, **3**, 816–821, https://doi.org/10.1038/nclimate1911.

Huang, J., H. Yu, X. Guan, G. Wang, and R. Guo, 2015: Accelerated dryland expansion under climate change. *Nat. Climate Change*, **6**, 166–171, https://doi.org/10.1038/nclimate2837.

Kochendorfer, J., and Coauthors, 2017a: The quantification and correction of wind-induced precipitation measurement errors. *Hydrol. Earth Syst. Sci.*, **21**, 1973–1989, https://doi.org/10.5194/hess-21-1973-2017.

——, and Coauthors, 2017b: Analysis of single-alter-shielded and unshielded measurements of mixed and solid precipitation from WMO-SPICE. *Hydrol. Earth Syst. Sci.*, **21**, 3525–3542, https://doi.org/10.5194/hess-21-3525-2017.

——, and Coauthors, 2018: Testing and development of transfer functions for weighing precipitation gauges in WMO-SPICE. *Hydrol. Earth Syst. Sci.*, **22**, 1437–1452, https://doi.org/10.5194/hess-22-1437-2018.

Lanza, L., M. Leroy, J. van der Meulen, and M. Ondras, 2005: The WMO laboratory intercomparison of rainfall intensity gauges, instruments and observing methods. WMO/TD-82, 139 pp., https://www.wmo.int/pages/prog/www/IMOP/reports/2003-2007/RI-IC_Final_Report.pdf.

Lanza, L. G., and E. Vuerich, 2009: The WMO field intercomparison of rain intensity gauges. *Atmos. Res.*, **94**, 534–543, https://doi.org/10.1016/j.atmosres.2009.06.012.

——, and L. Stagi, 2012: Non-parametric error distribution analysis from the laboratory calibration of various rainfall intensity gauges. *Water Sci. Technol.*, **65**, 1745–1752, https://doi.org/10.2166/wst.2012.075.

Leeper, R. D., M. A. Palecki, and E. Davis, 2015: Methods to calculate precipitation from weighing-bucket gauges with redundant depth measurements. *J. Atmos. Oceanic Technol.*, **32**, 1179–1190, https://doi.org/10.1175/JTECH-D-14-00185.1.

Nelder, J. A., and R. Mead, 1965: A simplex method for function minimization. *Comput. J.*, **7**, 308–313, https://doi.org/10.1093/comjnl/7.4.308.

Nešpor, V., and B. Sevruk, 1999: Estimation of wind-induced error of rainfall gauge measurements using a numerical simulation. *J. Atmos. Oceanic Technol.*, **16**, 450–464, https://doi.org/10.1175/1520-0426(1999)016<0450:EOWIEO>2.0.CO;2.

Nitu, R., and K. Wong, 2010: CIMO survey on national summaries of methods and instruments for solid precipitation measurement at automatic weather stations. WMO Instruments and Observing Methods Rep. 102, WMO/TD-1544, 57 pp., https://www.wmo.int/pages/prog/www/IMOP/publications/IOM-102_SolidPrecip.pdf.

——, and Coauthors, 2018: WMO Solid Precipitation Intercomparison Experiment (SPICE) (2012 - 2015). Instruments and Observing Methods Rep. 131, 1445 pp., https://library.wmo.int/doc_num.php?explnum_id=5686.

Pierre, A., S. Jutras, C. Smith, J. Kochendorfer, V. Fortin, and F. Anctil, 2019: Evaluation of catch efficiency transfer functions for unshielded and single-alter-shielded solid precipitation measurements. *J. Atmos. Oceanic Technol.*, **36**, 865–881, https://doi.org/10.1175/JTECH-D-18-0112.1.

Rasmussen, R., and Coauthors, 2012: How well are we measuring snow: The NOAA/FAA/NCAR winter precipitation test bed. *Bull. Amer. Meteor. Soc.*, **93**, 811–829, https://doi.org/10.1175/BAMS-D-11-00052.1.

Reverdin, A., M. Earle, A. Gaydos, and M. A. Wolff, 2016: Description of the quality control and event selection procedures used within the WMO-SPICE project. *Proc. WMO Tech. Conf. on Meteorological and Environmental Instruments and Methods of Observation*, Madrid, Spain, WMO, P3.10, https://www.wmocimo.net/eventpapers/session3/posters3/P3(10)_Reverdin.pdf.

Savina, M., B. Schäppi, P. Molnar, P. Burlando, and B. Sevruk, 2012: Comparison of a tipping-bucket and electronic weighing precipitation gage for snowfall. *Atmos. Res.*, **103**, 45–51, https://doi.org/10.1016/j.atmosres.2011.06.010.

Schewe, J., and Coauthors, 2014: Multimodel assessment of water scarcity under climate change. *Proc. Natl. Acad. Sci. USA*, **111**, 3245–3250, https://doi.org/10.1073/pnas.1222460110.

Sevruk, B., M. Ondrás, and B. Chvíla, 2009: The WMO precipitation measurement intercomparisons. *Atmos. Res.*, **92**, 376–380, https://doi.org/10.1016/j.atmosres.2009.01.016.

Smith, C. D., D. Yang, A. Ross, and A. Barr, 2019a: The environment and climate change Canada solid precipitation intercomparison data from Bratt's Lake and Caribou Creek, Saskatchewan. *Earth Syst. Sci. Data*, **11**, 1337–1347, https://doi.org/10.5194/essd-11-1337-2019.

——, A. Ross, J. Kochendorfer, M. E. Earle, M. Wolff, S. Buisán, Y.-A. Roulet, and T. Laine, 2019b: Evaluation of the WMO-SPICE transfer functions for adjusting the wind bias in solid precipitation measurements. *Hydrol. Earth Syst. Sci. Discuss.*, https://doi.org/10.5194/HESS-2019-313 .

Sugiura, K., D. Q. Yang, and T. Ohata, 2003: Systematic error aspects of gauge-measured solid precipitation in the Arctic, Barrow, Alaska. *Geophys. Res. Lett.*, **30**, e2019GL086357, https://doi.org/10.1029/2002GL015547.

Sypka, P., 2019: Dynamic real-time volumetric correction for tipping-bucket rain gauges. *Agric. For. Meteor.*, **271**, 158–167, https://doi.org/10.1016/j.agrformet.2019.02.044.

Thériault, J. M., R. Rasmussen, K. Ikeda, and S. Landolt, 2012: Dependence of snow gauge collection efficiency on snowflake characteristics. *J. Appl. Meteor. Climatol.*, **51**, 745–762, https://doi.org/10.1175/JAMC-D-11-0116.1.

Trenberth, K. E., 2011: Changes in precipitation with climate change. *Climate Res.*, **47**, 123–138, https://doi.org/10.3354/cr00953.

——, A. Dai, R. M. Rasmussen, and D. B. Parsons, 2003: The changing character of precipitation. *Bull. Amer. Meteor. Soc.*, **84**, 1205–1218, https://doi.org/10.1175/BAMS-84-9-1205.

Wolff, M., K. Isaksen, R. Braekkan, E. Alfnes, A. Petersen-Overleir, and E. Ruud, 2013: Measurements of wind-induced loss of solid precipitation: Description of a Norwegian field study. *Hydrol. Res.*, **44**, 35–43, https://doi.org/10.2166/nh.2012.166.

——, ——, A. Petersen-Overleir, K. Odemark, T. Reitan, and R. Braekkan, 2015: Derivation of a new continuous adjustment function for correcting wind-induced loss of solid precipitation: Results of a Norwegian field study. *Hydrol. Earth Syst. Sci.*, **19**, 951–967, https://doi.org/10.5194/hess-19-951-2015.